



Lead acetate trihydrate precursor route to synthesize novel ultrafine lead oxide from spent lead acid battery pastes



Xiaojuan Sun ^{a, b, 1}, Jiakuan Yang ^{a, b, *}, Wei Zhang ^a, Xinfeng Zhu ^{a, c}, Yuchen Hu ^a, Danni Yang ^a, Xiqing Yuan ^a, Wenhao Yu ^a, Jinxin Dong ^a, Haifeng Wang ^a, Lei Li ^a, R. Vasant Kumar ^d, Sha Liang ^{a, 1}

^a School of Environmental Science and Engineering, Huazhong University of Science and Technology (HUST), 1037 Luoyu Road, Wuhan, Hubei 430074, PR China

^b Key Laboratory for Large-Format Battery Materials and System of Ministry of Education, Huazhong University of Science & Technology, (HUST), 1037 Luoyu Road, Wuhan, Hubei 430074, PR China

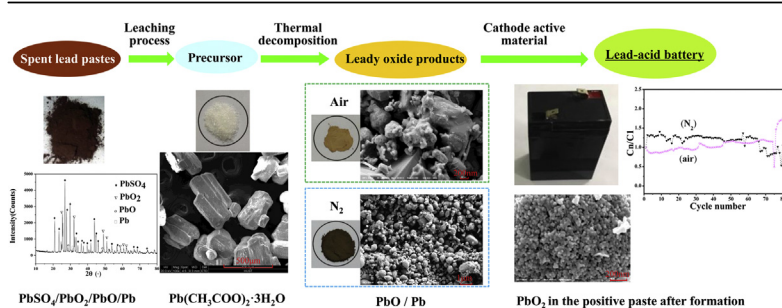
^c Henan University of Urban Construction, Pingdingshan, Henan 467000, PR China

^d Department of Materials Science and Metallurgy, University of Cambridge, Cambridge CB2 3QZ, UK

HIGHLIGHTS

- The $\text{Pb}(\text{CH}_3\text{COO})_2 \cdot 3\text{H}_2\text{O}$ precursor was prepared from the spent lead battery pastes.
- Novel lead oxide products were prepared from the precursor in N_2 and air.
- The assembled batteries show a good cyclic stability in 80 charge/discharge cycles.

GRAPHICAL ABSTRACT



ARTICLE INFO

Article history:

Received 16 April 2014

Received in revised form

6 June 2014

Accepted 1 July 2014

Available online 14 July 2014

Keywords:

Spent lead acid battery
Novel ultrafine lead oxide
Lead acetate trihydrate
Thermal decomposition
Electrochemistry test

ABSTRACT

A novel green recycling process is investigated to prepare lead acetate trihydrate precursors and novel ultrafine lead oxide from spent lead acid battery pastes. The route contains the following four processes. (1) The spent lead pastes are desulphurized by $(\text{NH}_4)_2\text{CO}_3$. (2) The desulphurized pastes are converted into lead acetate solution by leaching with acetic acid solution and H_2O_2 ; (3) The $\text{Pb}(\text{CH}_3\text{COO})_2 \cdot 3\text{H}_2\text{O}$ precursor is crystallized and purified from the lead acetate solution with the addition of glacial acetic acid; (4) The novel ultrafine lead oxide is prepared by the calcination of lead acetate trihydrate precursor in N_2 or air at 320 – 400 °C. Both the lead acetate trihydrate and lead oxide products are characterized by TG-DTA, XRD, and SEM techniques. The calcination products are mainly α -PbO, β -PbO, and a small amount of metallic Pb. The particle size of the calcination products in air is significantly larger than that in N_2 . Cyclic voltammety measurements of the novel ultrafine lead oxide products show good reversibility and cycle stability. The assembled batteries using the lead oxide products as cathode active materials show a good cyclic stability in 80 charge/discharge cycles with the depth of discharge (DOD) of 100%.

© 2014 Elsevier B.V. All rights reserved.

* Corresponding author. School of Environmental Science and Engineering, Huazhong University of Science and Technology (HUST), 1037 Luoyu Road, Wuhan, Hubei 430074, PR China. Tel./fax: +86 27 87792207.

E-mail addresses: jkyang@mail.hust.edu.cn, yjiakuan@hotmail.com (J. Yang).

¹ These two authors contributed equally to this paper.

1. Introduction

Globally, lead-acid battery constitutes the largest volume among secondary batteries arising from the advantages of low cost, good

stability, and high recovery ratio of over 97% of the spent batteries. Lead acid batteries account for nearly 80 wt% of the total lead consumption [1–3]. While the recovery of spent lead-acid battery is the most successful example among all commercial batteries throughout the world, any contamination during discarding, recovery or recycling the spent lead-acid batteries has drawn serious attention due to their toxicity to the environment [4–6]. A typical spent lead acid battery mainly consists of four components: spent electrolyte (11–30 wt %), lead alloy grid (24–30 wt %), lead pastes (30–40 wt %), and polymeric materials (22–30 wt %) [7]. Among these, lead paste is the most difficult to deal with because of the presence of active lead compounds in relatively stable state. A typical composition of a spent paste is lead sulphate (nearly 60%), lead (IV) dioxide (nearly 28%), lead (II) oxide (nearly 9%), metallic lead (nearly 3%) and a small but significant concentration of impurities such as iron, antimony, tin and barium [7,8]. Environmentally sensitive recovery of spent lead-acid battery pastes has attracted considerable interest from researchers [9–11].

The traditional pyrometallurgical route, which is the most widely used in the recovery of secondary lead resource, can emit large quantities of SO_2 gas and lead dust, causing threat to the environment [12–14]. Moreover, the pyrometallurgical process requires a lot of energy for the decomposition of lead sulfate above 1000 °C, thus it will consume non-renewable resources of coal, coke, oil or natural gas.

More recently increasing attention has been paid to the recovery of spent lead-acid battery pastes through alternative hydrometallurgical process. The most used hydrometallurgy method, which consists of pretreatment, desulfurization, reduction and electro-winning process, can avoid SO_2 and lead dust emission problems [15,16]. However, the energy efficiency of electro-winning process is low, with a higher total energy consumption compared with traditional pyrometallurgical route. The suggested leaching solutions of H_2SiF_6 or HBF_4 can lead to emission of fluorine in the environment which is also unacceptable.

Given the disadvantages in the traditional pyrometallurgical and electro-winning methods, several new hydrometallurgy approaches have been developed. Attempts have been tried to leach the components (PbSO_4 , PbO_2 and PbO) of spent lead pastes by citric acid and sodium citrate as reported in our previous studies [10,11,17]. In this leaching process, the lead citrate precursor is separated from the leaching solution by simple crystallization. The ultra-fine lead oxide powder can be obtained through calcination of lead citrate at a temperatures less than 400 °C. In order to improve the desulfurization efficiency of spent lead pastes, spent lead pastes were firstly converted into the desulfurized pastes with desulfurizing agents, then the desulfurized pastes were leached with citric acid solution to generate lead citrate [18]. In order to improve the speed of leaching reaction and decrease the consumption of citric acid, a modified version using acetic acid and sodium citrate leaching system was developed for the recovery of spent lead pastes [19]. However, in these previous researches, the impurities in spent lead pastes can easily join and contaminate the lead citrate precursor, leading sometimes to an unacceptably high content of the impurities in the final leady oxide. And then, the capacity retention ratio of the batteries manufactured with the leady oxide as the active material of the cathode decreases rapidly after 20–30 cycles. The impurities in the leady oxides could lead to the deterioration of the cycle life performance of the batteries [20]. Moreover, the leaching agents of citric acid and sodium citrate are relative more expensive than other organic or inorganic acids.

The objective of this work was to seek a more efficient method to obtain high-performance leady oxide with lower content of impurities by applying high-purity lead acetate trihydrate as a

precursor. Flow sheet of this process was schematically shown in Fig. 1. The suggested method can be described as “paste to paste” recycling. In this novel approach, the high-cost leaching reagents of citric acid and sodium citrate were substituted by the cheaper acetic acid. Furthermore, the impurities in spent pastes could be effectively separated by the three filtering-separating procedures. The morphology, mineral phases and electrochemical performances of lead oxide products prepared in N_2 or air were characterized, and batteries were fabricated by the new lead oxide products to examine the battery performance.

2. Experimental

2.1. Reactants and raw materials

The samples of spent lead acid battery pastes were provided by Hubei Jinyang Metallurgical Co. Ltd., China, where typically spent lead battery pastes are pyrometallurgically treated to recover lead as a metal using a conventional smelting process. Lead pastes from the spent lead-acid batteries were made available for this work after a separation process using Engitec Technologies Company CX

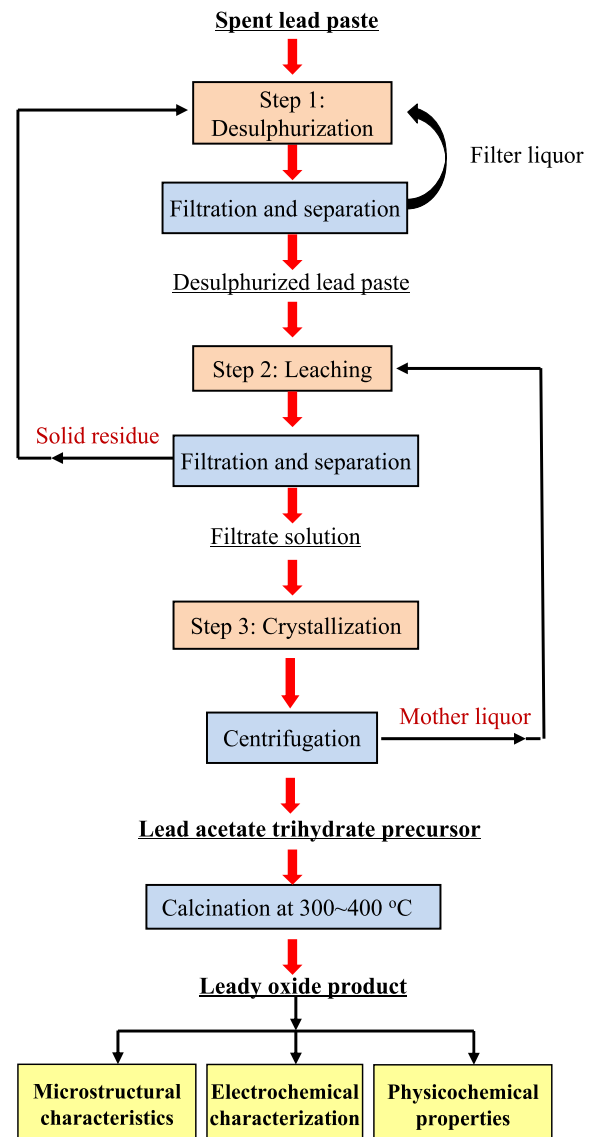


Fig. 1. Flow-sheet of the new hydrometallurgical process for recovery of lead pastes.

crushing and sorting system. The lead paste samples were washed with distilled water until pH of the washed water was above 6.5. Dried lead paste powders which passed through 120-mesh screens were used as raw materials in this study. The chemical compositions of lead and main metallic element in the used lead pastes are shown in Table 1. The antimony in spent lead-acid battery grid may enter into lead paste during the crushing process in the sorting system. Since the crushing and sorting equipment is made of iron and steel, Fe as an impurity can easily enter into the lead paste. For chemical analysis, the lead paste sample was digested by nitric acid, and Inductively Coupled Plasma Atomic Emission Spectroscopy (Optima4300DV, USA) was used to determine the contents of main metallic elements in the paste.

An aqueous solution of ammonium carbonate ((NH₄)₂CO₃, 99% purity, Sinopharm Chemical Reagent Co., Ltd, China) was used as the desulphurizing agent to react with PbSO₄ in the lead pastes. Aqueous solution of acetic acid (CH₃COOH, 99% purity, Sinopharm Chemical Reagent Co., Ltd, China) was used as the leaching agent to react with lead in the desulphurized paste. Hydrogen peroxide (H₂O₂, 30%W/V, Sinopharm Chemical Reagent Co., Ltd, China) was used as a reducing agent in order to reduce lead (IV) dioxide into lead (II) oxide in the lead pastes and render leachability of the PbO₂ phase.

2.2. Desulphurization of spent lead paste

100.0 g of the separated lead paste sample was added into a solution of (NH₄)₂CO₃, and reacted at a constant stirring speed of 450 rpm for 4 h. According to our previous study [7], the optimum dosage of (NH₄)₂CO₃ is found to be 32.0 g with a molar ratio of (NH₄)₂CO₃ to PbSO₄ in the lead pastes of 2:1, while the dosage of the distilled water is 500.0 g at the mass ratio of water to the lead

pastes were reacted with the leaching solution containing acetic acid and hydrogen peroxide. Only a small amount of un-reacted solid components remained, which were filtered and separated from the leaching solution. The leaching experiments were conducted in triplicate, and the mean values were calculated. The filtrate was collected for the next step in the overall procedure.

The leaching efficiency for lead in desulphurized lead paste was calculated by Equation (1):

$$\text{Leaching efficiency of lead} = (V_1 \times C_2) / (W_1 \times C_1) \times 100\% \quad (1)$$

In Equation (1), W₁ (g) is the mass of the desulphurized lead pastes; V₁ (L) is the volume of filtrate solution. C₁ (wt %) is the mass percent of lead in the desulphurized lead pastes, C₂ (g L⁻¹) is the lead concentration in the filtrate solution. The concentration of lead in the digestion solution of desulphurized lead pastes and filtrate solution was measured by AAS (novAA400, Analytik Jena AG).

2.4. Synthesis of Pb(CH₃COO)₂·3H₂O from the filtrate after the leaching process

The glacial acetic acid was then added to a 50 mL solution of the collected filtrate to crystallize Pb(CH₃COO)₂·3H₂O from the mother liquor. Thus crystal could be filtered and separated from the mother liquor of the filtrate, since most of impurities comprising Fe, Sb, and Cu, etc. were soluble and retained in the mother liquor. At different molar ratios of glacial acetic acid to lead in the collected filtrate (expressed as CH₃COOH/Pb_{in the filtrate}), the yield efficiency of Pb(CH₃COO)₂·3H₂O product and the pH of mother liquor were determined. The yield efficiency of Pb(CH₃COO)₂·3H₂O product was calculated by Equation (2):

$$\text{Yield efficiency of Pb(CH}_3\text{COO)}_2 \cdot 3\text{H}_2\text{O product (\%)} = \frac{\text{The mass of Pb(CH}_3\text{COO)}_2 \cdot 3\text{H}_2\text{O product (g)}}{\text{Stoichiometric maximum yield of Pb(CH}_3\text{COO)}_2 \cdot 3\text{H}_2\text{O product (g)}} \times 100\% \quad (2)$$

paste (L/S) of 5:1. After the desulphurization and the filtration process, the solid cake was washed with distilled water and collected. Nearly 93.2 g desulphurized lead pastes were obtained for the next leaching step. The amount of un-converted S in the desulphurized pastes was analyzed by using a High-frequency Infrared Carbon & Sulfur Analyzer (HCS-140, Shanghai DeKai Instrument Co., Ltd. China). The contents of PbSO₄, PbO₂, PbO and Pb components in the original and the desulphurized lead paste were determined by chemical analysis.

2.3. Leaching of the desulphurized lead paste with the acetic acid

The obtained 93.2 g desulphurized lead pastes were used in the following leaching procedure with 3 mol L⁻¹ acetic acid and 30%W/V H₂O₂ at a stirring speed of 400 rpm. Various molar ratios (0.75, 1.0, 1.5, 2, 2.5, and 3) of acetic acid to total Pb in desulphurized lead pastes, expressed as CH₃COOH/Pb, were investigated. After leaching for 6.0 h, almost all components in the solid desulphurized lead

2.5. Thermal analyses of Pb(CH₃COO)₂·3H₂O crystal precursor

The thermal analysis of crystal precursor was conducted by thermogravimetric – differential thermal analysis (TG-DTA) using Diamond (Platinum-Selmer equipment Co. Ltd., Shanghai), under air or nitrogen gas at a heating rate of 5 °C min⁻¹ from room temperature to 500 °C.

2.6. Calcination of Pb(CH₃COO)₂·3H₂O

Calcination temperature of Pb(CH₃COO)₂·3H₂O crystal was determined based on TG-DTA data. In N₂, the lead acetate precursors were calcinated at 205 °C, 265 °C, 320 °C, 370 °C and 400 °C for 1 h, at each temperature. In air, the lead acetate precursors were calcinated at 205 °C, 260 °C, 295 °C, 350 °C and 400 °C for 1 h, at each temperature.

2.7. Characterization of materials

Powder X-ray diffraction (XRD) data were collected from powder samples of Pb(CH₃COO)₂·3H₂O crystal product and the combustion products using a X'Pert PRO XRD (Philips, PAN alytical B.V., Holland) with Cu K α radiation and $\lambda = 1.5418 \text{ \AA}$ at scanning rate of 0.28° per second for 2 θ in the range from 5° to 75°.

Table 1

Chemical compositions of lead and other main metallic elements in the spent lead pastes (wt. %).

Compositions	Pb	Cu	As	Zn	Sb	Fe	Cd
Percentage (wt%)	76.600	0.008	0.040	0.003	0.240	0.100	0.002

Morphology studies were carried out with scanning electron microscopy (ULTRA PLUS-43-13, Germany) operated at 10 kV after coating the samples with gold. EDX spectra of the calcined products from lead acetate precursors were collected on an ultra-thin window (UTW) X-ray detector equipped with SEM.

2.8. Electrochemical measurements and physicochemical properties of lead oxide products

The cyclic voltammetry (CV) curves of lead oxide powder were determined with a three-electrode system [20,21]. The working electrode was a microelectrode filled with the tested lead oxide powder. The counter electrode was a double platinum electrode, while Hg/Hg₂SO₄/K₂SO₄ (sat.) was chosen as the reference electrode. The electrolyte was sulphuric acid solution at concentration of 3.0 mol L⁻¹. The CV tests were performed at room temperature (20 ± 2 °C) using VMP-2 device from USA at a scanning speed of 10 mV s⁻¹ in a potential range of 0 V to +1.5 V (anodic range), while the last 7 CV curves were collected from 20 cycles. The basic physicochemical properties of lead oxide powder product such as the degree of oxidation (oxidizability), density, acid-absorption and water-absorption values were determined according to our previous literature [20].

2.9. Battery assembling and testing procedure

The method of battery assembling and testing are based on our previous work reported in the literature [20]. In battery assembling, the lead oxide powder products act as positive active material, while negative plates were provided by Wuhan Changguang Power Sources. Co. Ltd. After the mixing and pasting, curing, and formation processes, each of the dried positive plates was coupled with two commercial negative plates soaked in sulphuric acid solution (1.335 g cm⁻³) electrolyte so that batteries for testing under 2 V/2 Ah could be made. The detailed parameters for the battery are provided in the [Supplementary File](#). Both the charging and the discharging cycle tests were performed repeatedly at a constant discharge current of 200 mA with a cut-off terminal voltage of 1.75 V (depth of discharge, DOD = 100%).

3. Results and discussion

3.1. Desulphurization of lead pastes by (NH₄)₂CO₃ solution

The chemical compositions of the original lead pastes and the desulphurized lead pastes are listed in [Table 2](#). As shown in [Table 2](#), nearly all of PbSO₄ component in the original lead paste was converted into PbCO₃ in the desulphurized lead paste. The amounts of other components such as PbO₂, PbO and Pb in the desulphurized lead paste remain more or less identical as in the original lead paste.

3.2. Leaching of desulphurized pastes by acetic acid solution and hydrogen peroxide

The effects of molar ratio of CH₃COOH/Pb on leaching efficiency of lead from the desulphurized pastes are presented in [Fig. 2](#).

Table 2

The comparison between chemical compositions of the original lead pastes and the desulphurized lead pastes (wt. %).

Specimen	PbCO ₃	PbSO ₄	PbO ₂	PbO	Pb	Others	Total Pb ^a
Original lead pastes	0.000	56.800	32.400	4.100	5.400	1.300	76.072
Desulphurized lead pastes	53.700	0.003	34.700	4.400	5.800	1.400	81.573

^a Total Pb is the mass ratio of total lead element to the mass of the lead paste.

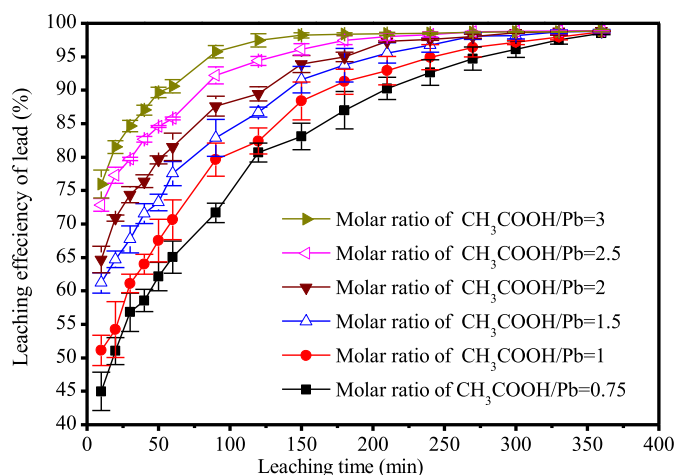
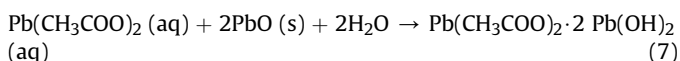
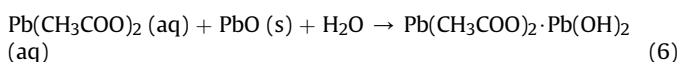
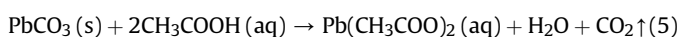
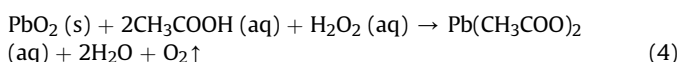


Fig. 2. Effect of molar ratio of CH₃COOH/Pb on leaching efficiency of Pb from the desulphurized pastes.

Generally, leaching efficiency of lead in the desulphurized pastes increased with the increase of molar ratio of CH₃COOH/Pb. It indicates that extraction efficiency of lead could reach up to over 95% at each molar ratio of CH₃COOH/Pb provided leaching time is long enough. Even at the minimum molar ratio of CH₃COOH/Pb of 0.75, the leaching efficiency of lead could also increase up to nearly 97.6% for a leaching duration of 360 min. Therefore, it shows that the leaching efficiency of lead from the desulphurized lead paste is high with the leaching system of acetic acid and hydrogen peroxide solution. The solid residue in the desulphurized lead pastes after the leaching process consisted of a small amount of un-converted PbSO₄ and other insoluble solid impurities.

The reactions of lead paste with acetic acid solution and H₂O₂ might be presented as indicated in the following Equations (3)–(7).



With the addition of acetic acid solution and hydrogen peroxide, a large number of gas bubbles are observed to emit in the stirring vessel due to the generation of oxygen and carbon dioxide as shown in Equations (4) and (5).

When the molar ratio of CH₃COOH/Pb was 0.75, the concentration of lead and pH of the solution after leaching for the different extended durations are shown in [Fig. 3](#). The concentration of lead increased from 1.60 to 3.95 mol L⁻¹ when the leaching time is increased from 10 to 360 min. The pH value simultaneously increased from 4.27 to 8.12, indicating that the acetic acid solution was almost completely consumed and reacted with the desulphurized paste.

3.3. Crystallization of Pb(CH₃COO)₂·3H₂O crystal

The XRD pattern of the crystal product is shown in [Fig. 4](#) (a), while photographic and SEM images are shown in [Fig. 4](#)(b) and (c).

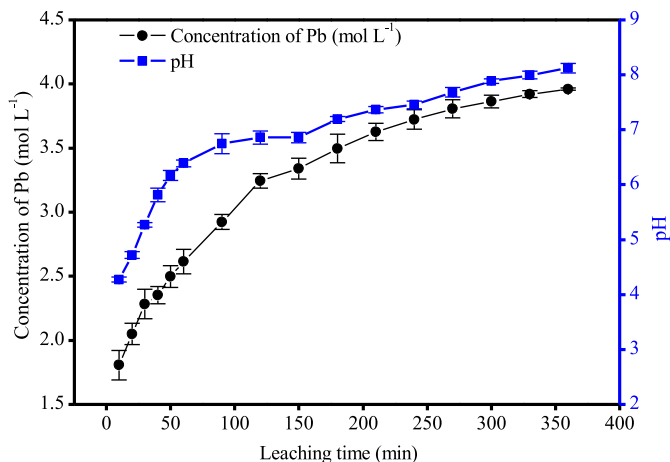
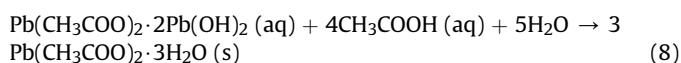


Fig. 3. Effect of leaching time on concentration of Pb and pH in the leaching solution at the molar ratio of CH₃COOH/Pb of 0.75.

The product was identified as Pb(CH₃COO)₂·3H₂O (JCPDS No. 00-014-0829). Thus, the reaction of glacial acetic acid and the lead acetate filtrate solution may be expressed as the Equation (8).



The effects of CH₃COOH/Pb_{in the filtrate} on yield efficiency of Pb(CH₃COO)₂·3H₂O crystal and pH in the solution are shown in Fig. 5. As shown in Fig. 5, the mass of the Pb(CH₃COO)₂·3H₂O crystal product increased when CH₃COOH/Pb_{in the filtrate} increased. The yield efficiency of Pb(CH₃COO)₂·3H₂O crystal can reach up to nearly 85.0% at a molar ratio of CH₃COOH/Pb_{in the filtrate} of 1.4 and then remained constant with any further increase of the molar ratio of

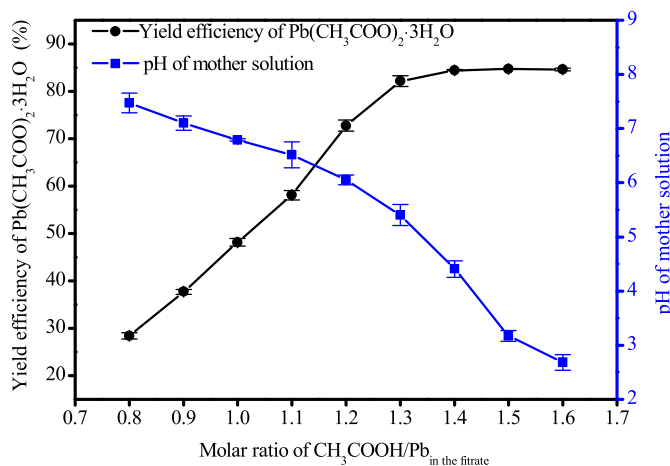


Fig. 5. Effect of molar ratio of CH₃COOH/Pb in the filtrate on yield efficiency of Pb(CH₃COO)₂·3H₂O product and pH in the mother solution.

CH₃COOH/Pb_{in the filtrate}. The pH of lead acetate solution decreased from 7.6 to 2.8 with the molar ratio of CH₃COOH/Pb_{in the filtrate} increased from 0.8 to 1.6. It indicated that nearly 85.0% of lead was crystallized from the mother liquor with the formation of Pb(CH₃COO)₂·3H₂O.

3.4. Thermal analysis of the Pb(CH₃COO)₂·3H₂O product

The TG-DTA curves of lead acetate trihydrate in air and N₂ are shown in Fig. 6. According to Fig. 6, the mass loss of lead acetate

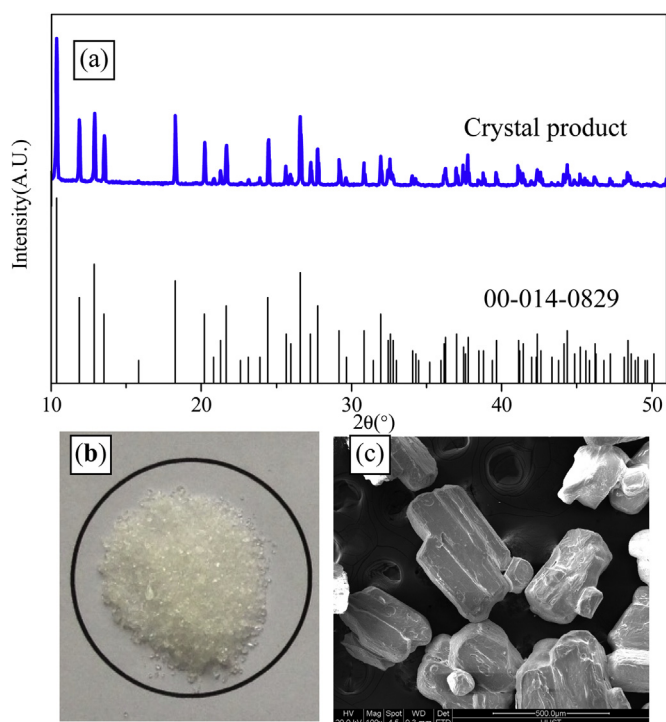


Fig. 4. The XRD pattern (a), Photograph (b) and SEM image (c) of the crystal product Pb(CH₃COO)₂·3H₂O.

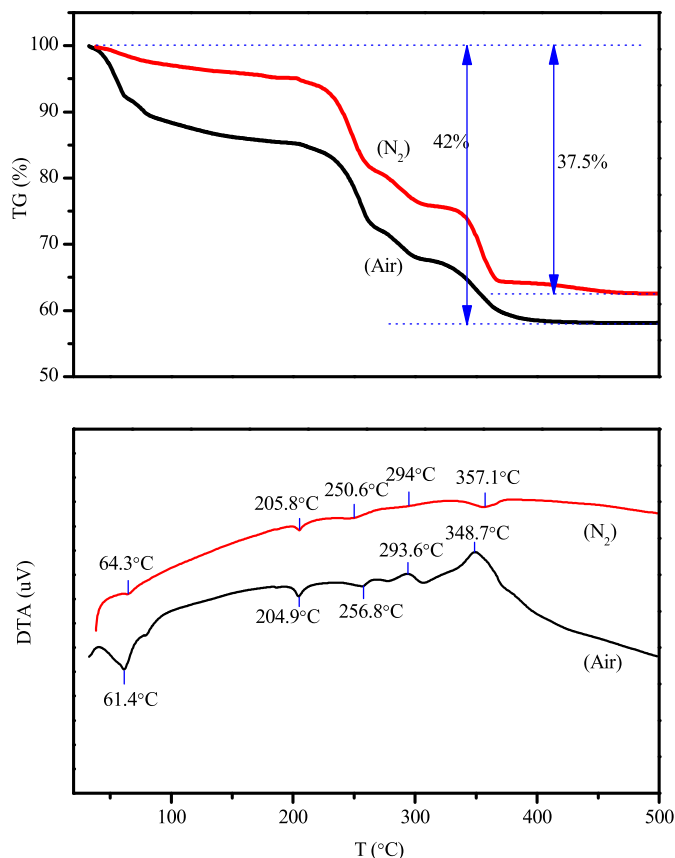


Fig. 6. TG-DTA curves of lead acetate trihydrate precursor in N₂ and air.



Fig. 7. The Photographs of products from lead acetate trihydrate precursor calcined in N_2 at different temperatures: (a) Original sample, (b) 205 °C, (c) 265 °C, (d) 320 °C, (e) 370 °C, and (f) 400 °C.

trihydrate in air (42.0%) was more than that in N_2 (37.5%). From the DTA curve in N_2 , there are five endothermic peaks at the temperatures of 64.3, 205.8, 250.6, 294, and 357.1 °C. It is indicated that lead acetate trihydrate undergoes a series of dehydrate and pyrolysis reactions which all are endothermic reaction in N_2 . While there are only three endothermic peaks at the temperature of 61.4, 204.9, 256.8 °C from the DTA curve in air; two exothermic peaks exist around 293.6 °C and 348.7 °C, which are ascribed to vigorous oxidation of C and organic matter when the temperature rises in air. The difference of thermal characteristics of lead acetate trihydrate in N_2 and in air is consistent with the XRD patterns of the calcination products from lead acetate trihydrate in N_2 and air. As shown in Fig. 8, a significant amount of $Pb(CH_3COO)_2$ and C are identified in the calcination products at 320 °C, which indicates that no exothermic oxidation reaction generates in N_2 . However, as shown in Fig. 11, no C, only a little amount of $Pb(CH_3COO)_2$, is identified in the calcination products at 295 and 350 °C, which indicates that exothermic oxidation reaction of C and intermediate

organic matter generates at the higher temperatures of about 295 °C in air.

3.5. Calcination products from lead acetate trihydrate in N_2

The photographs of lead oxide formed in N_2 are shown in Fig. 7. The original sample of lead acetate trihydrate precursor looks transparent and is a colorless crystal product, as shown in Fig. 7(a). The calcination products at 205 °C and 265 °C are white or grey powders, as shown in Fig. 7(b)–(c). Furthermore, the color of the calcination products turns into brown or dark when the calcination temperatures increase up to 320–400 °C, as shown in Fig. 7(d)–(f).

The XRD patterns of calcination products at different temperatures in N_2 for 1 h are shown in Fig. 8. The calcination products at 205 °C were found to be $Pb(CH_3COO)_2$ (JCPDS No: 00-043-0743), and $3Pb(CH_3COO)_2 \cdot PbO \cdot H_2O$ (JCPDS No: 00-018-1739). The calcination products at 265 °C were $Pb(CH_3COO)_2 \cdot 2PbO$ and $Pb(CH_3COO)_2 \cdot PbO$. The calcination products at 320 °C were mainly α -PbO, β -PbO, metallic Pb, carbon and some undecomposed $Pb(CH_3COO)_2$. With increasing calcination temperature, it was observed that the crystalline phases of the calcined products were transformed into α -PbO, β -PbO and metallic Pb. The calcination products at 370 °C and 400 °C were mainly α -PbO, β -PbO and metallic Pb as shown in the XRD patterns. Besides, diffraction peak intensity of α -PbO is stronger than that of β -PbO, indicating that the amount of α -PbO is more than that of β -PbO. From above analyses, the $Pb(CH_3COO)_2 \cdot 3H_2O$ precursor could be completely converted into PbO and Pb products at above 370 °C. The calcination reactions might be followed by Equations 9 and 10 in N_2 gas [22].

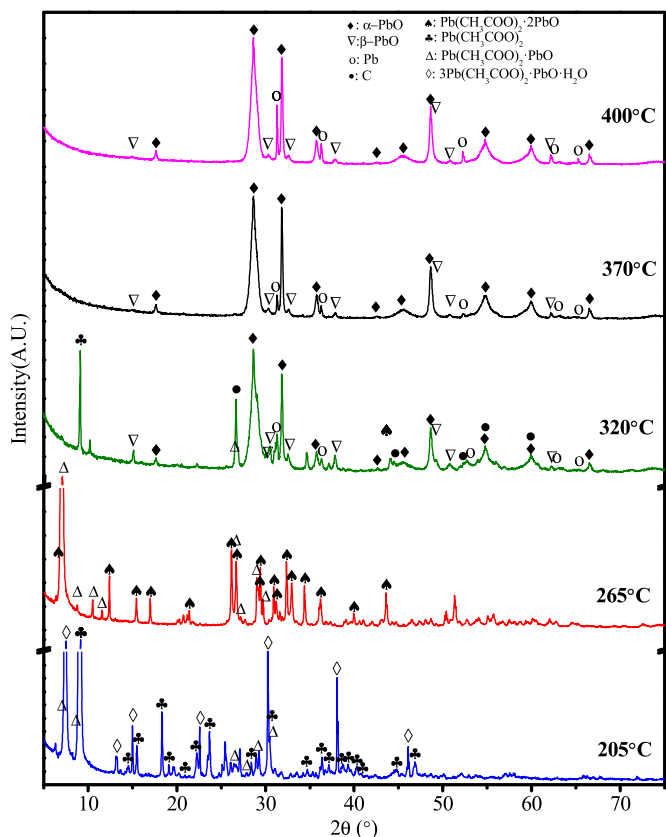
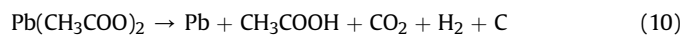


Fig. 8. The XRD patterns of calcination products from lead acetate trihydrate precursor in N_2 at different temperatures for 1 h: 205 °C, 265 °C, 320 °C, 370 °C, and 400 °C.

The SEM images of the calcination products at different temperatures in N_2 are shown in Fig. 9. As shown in Fig. 9(a) and (b), the products show plate-like shape in the size of 10–20 μm at the calcination temperatures of 205 °C and 265 °C. In Fig. 9(c), some spherical particles of size range 200–400 nm appear at 320 °C. In Fig. 9(d) and (e), the calcination products become uniform spherical particles of 200–400 nm at 370 and 400 °C, and some larger spherical particles show the tendency of agglomeration at the higher calcination temperature of 400 °C. In general, the morphologies of the products calcinated in N_2 change from plate-like shape into spherical shape when the temperature rises from 205 °C to 400 °C. The EDX spectra of the calcination product at 400 °C in N_2 shows that the major phase is identified as lead oxide, which is consistent with the XRD results in Fig. 8.

3.6. Calcination products from lead acetate trihydrate in air

The photographs of lead oxide products in air are shown in Fig. 10. As shown in Fig. 10, the calcination products at 205 °C are

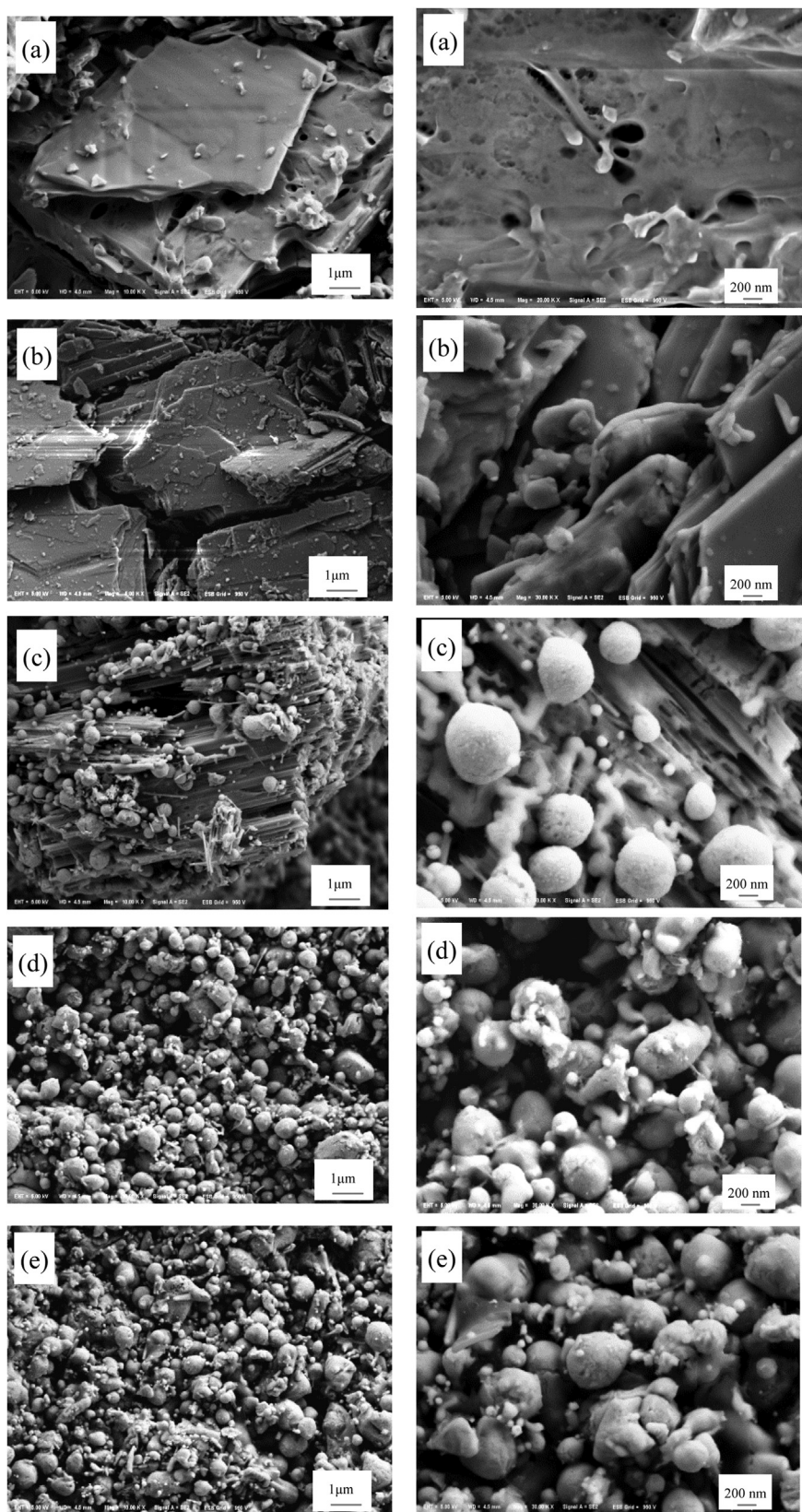


Fig. 9. The SEM images of calcination products from lead acetate trihydrate precursor in N_2 gas at different temperatures for 1 h: (a) 205 °C, (b) 265 °C, (c) 320 °C, (d) 370 °C, and (e) 400 °C.

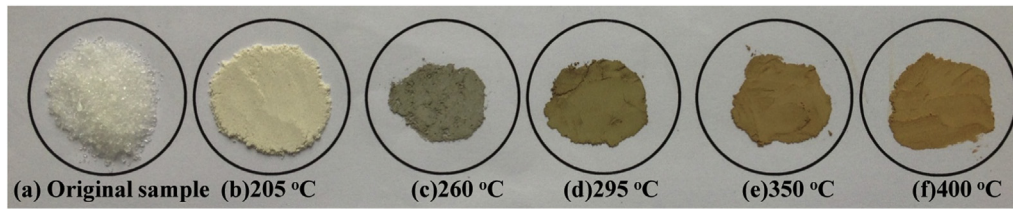


Fig. 10. The photographs of products from lead acetate calcined in air at different temperatures for 1 h: (a) Original sample, (b) 205 °C, (c) 260 °C, (d) 295 °C, (e) 350 °C, and (f) 400 °C.

white or grey powders, which is similar to the products calcinated at 205 °C in N₂. As shown in Fig. 10(c)–(f), the colors of the calcination products turn into grey or yellow when the calcination temperatures rise up to 260–400 °C, which is much different from brown or dark color of the products calcinated at corresponding temperatures in N₂. The color difference of calcination products mainly results from presence of C and intermediate organic matter in the calcination products in N₂. The color of lead oxide products turns to brown or dark since an amount of C residues are kept in the calcined products in N₂. However, much less C residue is kept in the calcined products in air since C is easily to oxidize with air.

The XRD patterns of calcination–combustion products at different temperatures in air are shown in Fig. 11. Similar to that in N₂, the products were mainly Pb(CH₃COO)₂, 3Pb(CH₃COO)₂·PbO·H₂O, and Pb(CH₃COO)₂·PbO at the calcination of 205 °C. The calcination products at 260 °C were Pb(CH₃COO)₂·2PbO and Pb(CH₃COO)₂·PbO. The calcination–combustion products at 295 °C were mainly α-PbO, β-PbO, metallic Pb, and a small amount of un-

combusted Pb(CH₃COO)₂. At higher temperature of 350 °C and 400 °C, the products were completely transformed into the phases of α-PbO, β-PbO and metallic Pb. The diffraction peak intensity of α-PbO is equal to that of β-PbO, indicating that the amount of α-PbO is approximately equal to that of β-PbO. Any existence of carbon as in air, is removed by oxidation by Equations 11–14:



Thus no carbon was identified in the calcined products in air.

The SEM images of the calcination–combustion products at different temperatures in air are shown in Fig. 12. Similar to that in N₂, the results show that the morphology is transformed from plate-like shape to a ball-like shape with increasing temperature. As shown in Fig. 12(a) and (b), the calcination–combustion products shows plate-like shape in the size of 10–20 μm at 205 °C and 265 °C. In Fig. 12(c), the calcination products are mainly particles of 200–400 nm, with a few undecomposed substances at 295 °C. In Fig. 12(d) and (e), two different kinds of spherical particles exist in the lead products, where fewer agglomerated spherical particles of 5 μm are dispersed in lots of smaller spherical particles of 400–800 nm at 350 °C and 400 °C. The EDX spectra of the calcination–combustion product at 400 °C shows that the major phase of calcination–combustion product is identified as lead oxide, which is consistent with the XRD results in Fig. 11.

3.7. Physicochemical properties and electrochemical characterization of lead oxide products

As shown from Table 3, the oxidizability of lead oxide products prepared in different calcination atmosphere is much higher than traditional ball-mill lead oxide products for which data was provided by Wuhan Changguang Power Sources. Co. Ltd. The oxidizability of lead oxide products prepared in N₂ is higher than in products in air with a small margin. As shown in Equations 11–14, the reduction reaction of PbO with solid carbon or CO gas in air atmosphere could result in the consumption of PbO, causing a lower oxidizability of lead oxide product in air than that in N₂.

The enhanced water absorption of lead oxide products may be due to smaller-sized structure of prepared products compared with traditional ball-mill lead oxide products since specific surface area of prepared products is much larger than traditional ball-mill products. The acid-absorption value is affected by the oxidizability of lead oxides and the particle size of lead oxides, because higher oxidizability and smaller particle size of lead oxide products result in higher acid-absorption value [20,23]. As shown in Table 3, the acid-absorption value of lead oxide products prepared with N₂

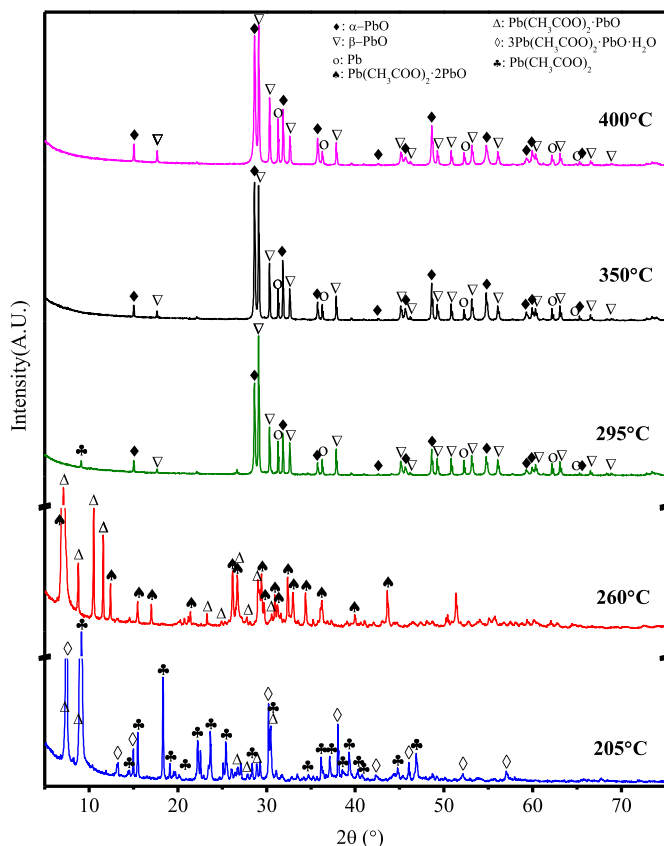


Fig. 11. The XRD patterns of calcination products from lead acetate trihydrate precursor in air at different temperatures for 1 h: 205 °C, 260 °C, 295 °C, 350 °C, 400 °C.

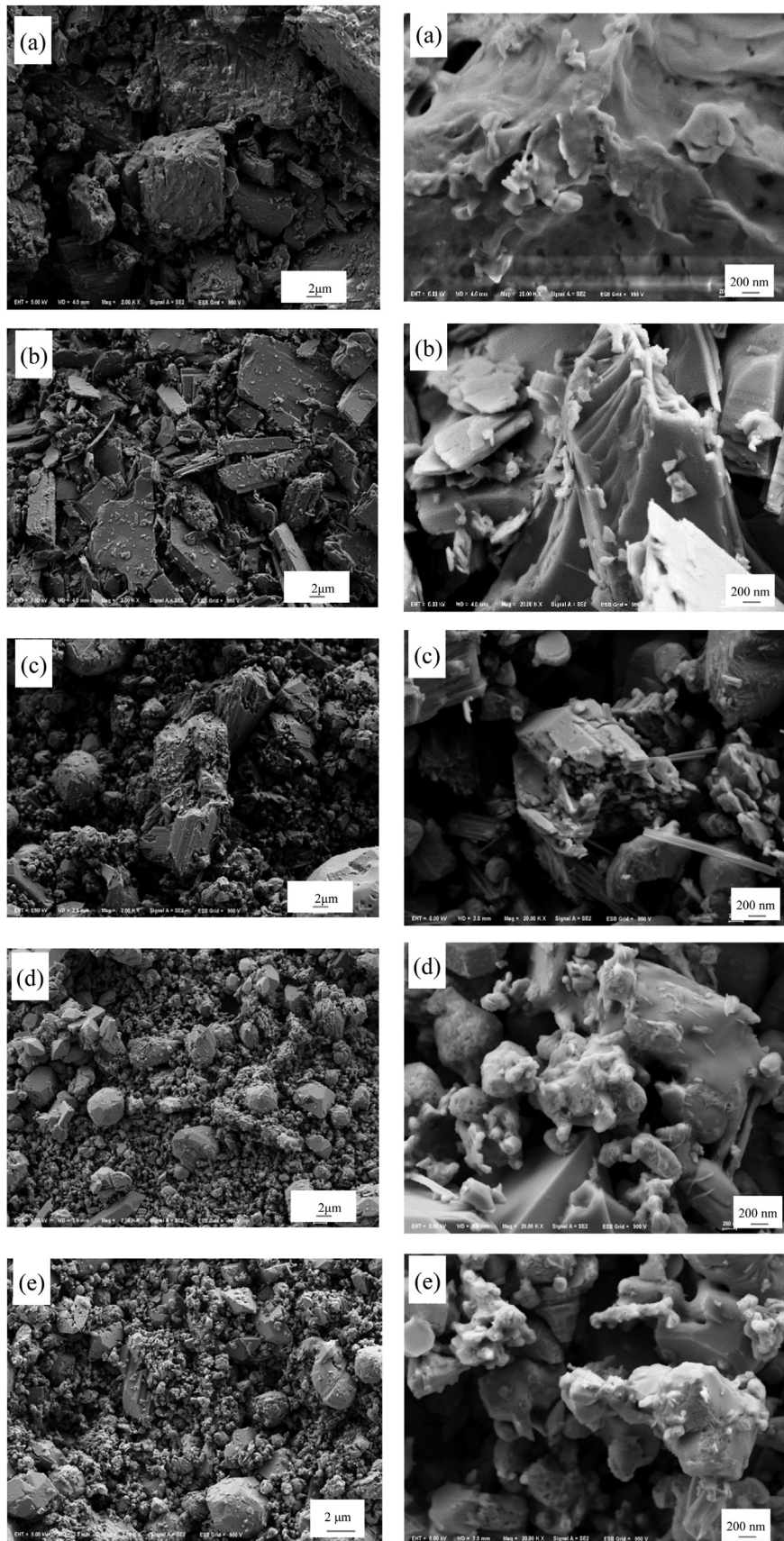


Fig. 12. The SEM images of calcination products from trihydrate precursor in air at different temperatures for 1 h: (a) 205 °C, (b) 260 °C, (c) 295 °C, (d) 350 °C, and (e) 400 °C.

Table 3
The physicochemical characteristics of different lead oxide products.

Calcination atmosphere	Calcination temperature/°C	Apparent density/g cm ⁻³	Degree of oxidation /%	Water-absorption value /ml kg ⁻¹	Acid-absorption value /g kg ⁻¹
N ₂	370	1.70	99.1	347.6	532.8
N ₂	400	1.68	99.2	352.0	554.2
Air	350	1.52	95.8	312.2	476.3
Air	400	1.47	96.0	332.7	492.6
Traditional leady oxide ^a		1.93	83.2	110.0	381.3

^a The traditional ball-mill leady oxide was provided by Wuhan Changguang Power Sources. Co. Ltd.

is higher than that with air. As shown in Figs. 9 and 12, the particle size of lead oxide products in N₂ is much smaller than in air, and the oxidizability of lead oxide products in N₂ is the maximum, which may contribute to the higher acid-absorption value of lead oxide products in N₂.

The last 7 CV curves in the CV tests of lead oxide prepared in N₂ (a) and air (b) are shown in Fig. 13. As shown in Fig. 13, the CV curves of the two kinds lead oxide product are similar, with four clear peaks and relatively stable peaks positions, indicating that the lead oxide product has good stability in electrochemical reactions.

The oxidization of PbO to α -PbO₂ which is described in peak (i) occurs at around +1.02 V(vs reference electrode), while oxidization of PbSO₄ to β -PbO₂ in peak (ii) occurs at around +1.3 V(vs reference electrode) [24,25]. Under the high potential, evolution of oxygen from the aqueous system takes place around +1.5 V (vs reference electrode), with the reaction being, 2H₂O → O₂ + 4H⁺ + 4e⁻. On the reverse scanning from potential +1.5 V, the reduction reaction of α -PbO₂ and β -PbO₂ to PbSO₄ occurs at about +0.9 V in peak (iii). The reduction peak (iii) in Fig. 13(b) is apparently larger than that of Fig. 13(a), which indicates a better charge and discharge performance of the lead oxide product prepared in air than that prepared in N₂. As shown in Fig. 14, the discharge capacity of two different products improved as cycle count increased, while lead oxide product prepared in air showed higher discharge capacity than that in N₂.

3.8. Battery performance

Fig. 15 shows the XRD patterns of plate samples made from lead oxide products in N₂ before and after the formation process. The

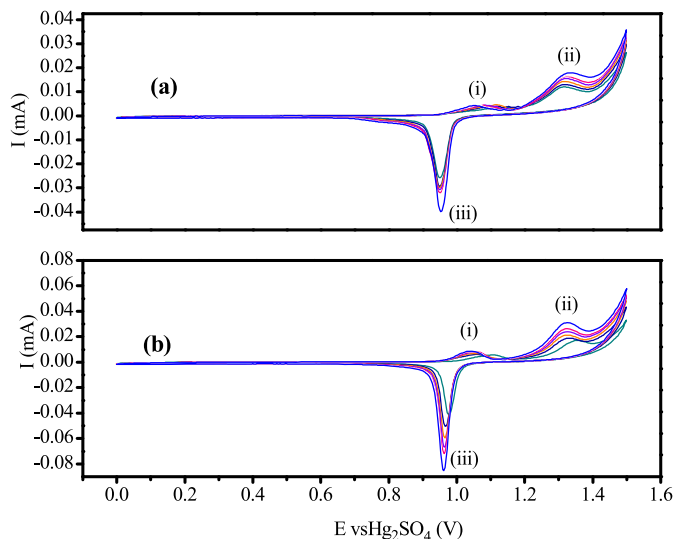


Fig. 13. The last 7 CV curves in all CV tests of the lead oxide specimens prepared in different atmosphere: (a) N₂ at 370 °C for 1 h, and (b) air at 350 °C for 1 h.

sample before the formation process mainly contains 4PbO·PbSO₄ (4BS) and α -PbO. The ripe plates after the formation process mainly comprise β -PbO₂, PbSO₄ and small amount of 3PbO·PbSO₄·H₂O (3BS). After the formation process, the main phase of plates turns into β -PbO₂. Fig. 16 shows the SEM images of plates made from lead oxide product prepared in N₂ gas before and after the formation process. As shown in Fig. 16(a), the plate before the formation process looks like the typical microstructure of 4BS and PbSO₄. However, the microstructure of the ripe plate shows fine spherical particles of β -PbO₂ with a diameter of 10–50 nm shown in Fig. 16(b).

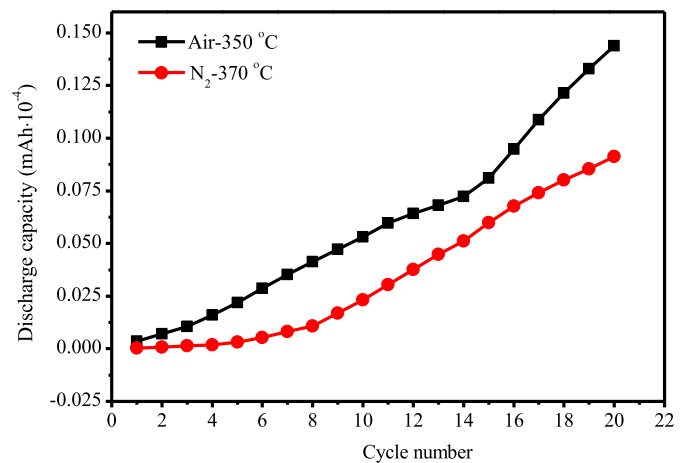


Fig. 14. Discharge capacity in the CV curves of calcination products prepared in air and N₂.

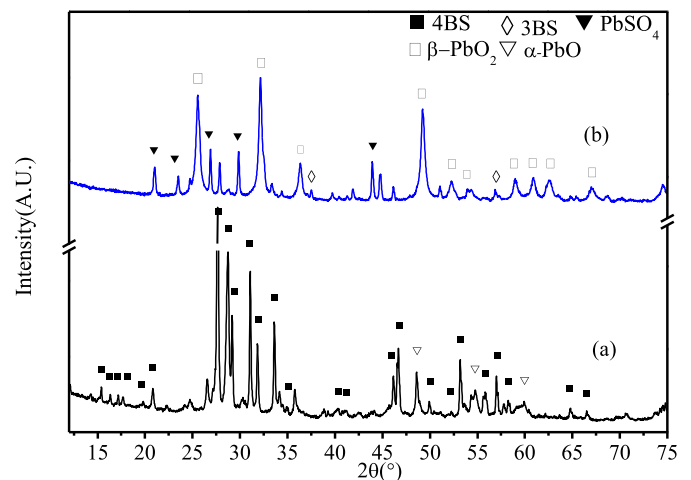


Fig. 15. The XRD patterns of plates made from lead oxide product prepared in N₂ at 375 °C: (a) before the formation process, and (b) after the formation process.

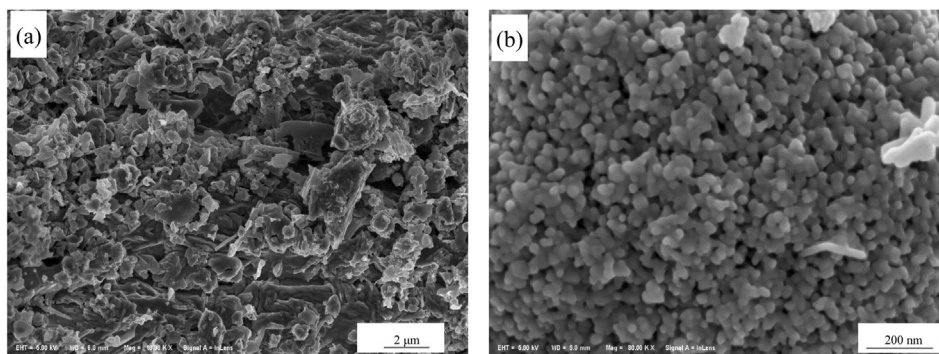


Fig. 16. The SEM images of the positive plate made from the lead oxide product prepared in N_2 at $375\text{ }^\circ\text{C}$: (a) before the formation process, and (b) after the formation process.

Cycle performance of batteries manufactured by lead oxide products in N_2 and air is shown in Fig. 17 (a) and (b), respectively. The capacity retention ratios of the assembling batteries made from the two kinds of lead oxide products show a good cyclic stability in 80 charge/discharge cycles with the depth of discharge (DOD) of 100%. The cycle performance of the assembled batteries in this study is significantly better than our previous study using the novel lead oxide recovered from the spent lead pastes with the acetic and sodium citrate leaching process. It might be related to lower concentration of impurities in the novel ultrafine lead oxide products with the lead acetate trihydrate precursor route than in the previous acetic and sodium citrate leaching route. Impurities in the recovered lead oxides have potential influences on the performance of the new lead-acid battery. In a further study we will investigate the typical impurities in the novel ultrafine lead oxide products, i.e., Fe, Sb, and Ba. The stable cycle performance may be due to favorable properties of lead oxide products in this method for the recovery of the spent lead-acid battery paste.

4. Conclusions

Pure $Pb(CH_3COO)_2 \cdot 3H_2O$ crystal has been prepared from spent lead acid battery pastes by desulphurization, leaching by acetic acid solution and crystallization procedure by glacial acetic acid. The $Pb(CH_3COO)_2 \cdot 3H_2O$ crystal is found to be pure, and can be readily separated from the mother liquor.

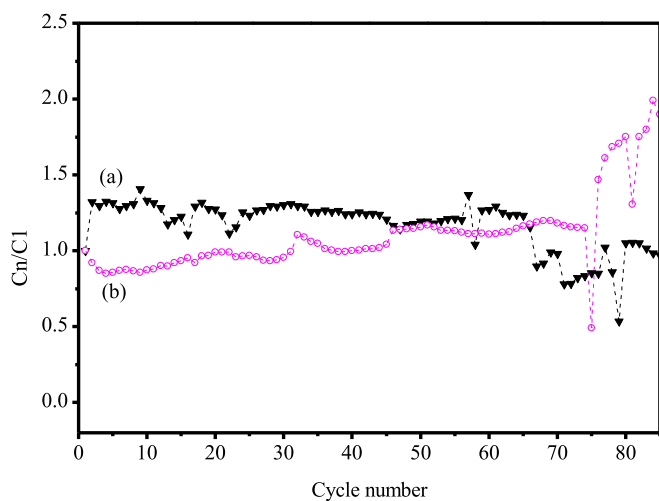


Fig. 17. The capacity retention ratio of the assembling batteries made from the lead oxide products prepared in different atmosphere: (a) N_2 at $370\text{ }^\circ\text{C}$ for 1 h, and (b) air at $350\text{ }^\circ\text{C}$ for 1 h.

The preparation of lead oxide product was carried out by calcining $Pb(CH_3COO)_2 \cdot 3H_2O$ crystal in N_2 or in air. In N_2 , the major phases of the calcination products at a temperature of above $320\text{ }^\circ\text{C}$ for 1 h were α -PbO, β -PbO, with a small amount of metallic Pb, and the amount of α -PbO is larger than that of β -PbO. The product morphology consisted of uniform spherical particles with a size range of 200–400 nm at typical calcinations temperatures of $370\text{ }^\circ\text{C}$ and $400\text{ }^\circ\text{C}$. In air, at the calcination temperature of over $295\text{ }^\circ\text{C}$ for 1 h the major phases of the products were still α -PbO, β -PbO, with a small amount of lead, and the amount of α -PbO is approximately equal to that of β -PbO. The morphology is converted from plate-like shape to spherical shape with increasing temperature. At the calcination temperature of $350\text{ }^\circ\text{C}$ and $400\text{ }^\circ\text{C}$, few larger agglomerated spherical particles of $5\text{ }\mu\text{m}$ are dispersed in a matrix of smaller spherical particles of 400–800 nm.

The basic physicochemical properties of lead oxide powder product show higher degree of oxidation, acid-absorption and water-absorption than traditional ball-mill lead oxide products, with lower apparent density. The CV curves of novel ultrafine lead oxide shows good reversible ability and cycle stability (above 20 cycles), and lead oxide product prepared in air exhibited higher electrochemical properties than that prepared in N_2 .

The assembled batteries made from the two kinds of lead oxide products prepared in both N_2 and air show a good cyclic stability in 80 charge/discharge cycles at a depth of discharge (DOD) of 100%.

Acknowledgments

The authors would like to express their thanks to the International Technology Cooperation Plan of Innovation Fund, HUST (2013ZZGH015), the Wuhan Planning Project of Science and Technology, China (2013060501010168, 2013011801010593, and 2014030709020313), and the national science and technology support program (2014BAC03B02). The authors would like to extend their thanks to Analytical and Testing Center of Huazhong University of Science and Technology (HUST) that supplied the facilities for materials analysis during this research. The authors would like to extend thanks to the raw materials and financial support from Hubei Jinyang Metallurgical Co. Ltd., China. We also show thanks to the support of Wuhan Changguang Power Sources Co. Ltd.

Appendix A. Supplementary data

Supplementary data related to this article can be found at <http://dx.doi.org/10.1016/j.jpowsour.2014.07.007>.

References

- [1] X. Zhu, J. Yang, L. Gao, J. Liu, D. Yang, X. Sun, W. Zhang, Q. Wang, L. Li, D. He, *Hydrometallurgy* 134 (2013) 47–53.
- [2] T. Blair, *J. Power Sources* 73 (1998) 47–55.
- [3] R.V. Kumar, J. Yang, M.S. Sonmez, *J. Powder Metall. Min.* 2 (2013) 1–5.
- [4] R. Kalahasthi, T. Barman, H.R. Rao, *J. Environ. Occup. Sci.* 1 (2012) 1–5.
- [5] L. Chen, Z. Xu, M. Liu, Y. Huang, R. Fan, Y. Su, G. Hu, X. Peng, *Sci. Total Environ.* 429 (2012) 191–198.
- [6] M. Haider, N. Qureshi, *Rocz. Panstw. Zakl. Hig.* 64 (2012) 37–42.
- [7] X. Zhu, L. Li, X. Sun, D. Yang, L. Gao, J. Liu, R.V. Kumar, J. Yang, *Hydrometallurgy* 117 (2012) 24–31.
- [8] T. Chen, J. Dutrizac, *Hydrometallurgy* 40 (1996) 223–245.
- [9] S. Maruthamuthu, T. Dhanibabu, A. Veluchamy, S. Palanichamy, P. Subramanian, N. Palaniswamy, *J. Hazard. Mater.* 193 (2011) 188–193.
- [10] M.S. Sonmez, R.V. Kumar, *Hydrometallurgy* 95 (2009) 82–86.
- [11] M.S. Sonmez, R.V. Kumar, *Hydrometallurgy* 95 (2009) 53–60.
- [12] M.A. Kreuzsch, M.J.J.S. Ponte, H.A. Ponte, N.M.S. Kaminari, C.E.B. Marino, V. Mymrin, *Resour. Conserv. Recycl.* 52 (2007) 368–380.
- [13] A. Bernardes, D.C.R. Espinosa, J.S. Tenório, *J. Power Sources* 130 (2004) 291–298.
- [14] N.K. Lyakov, D.A. Atanasova, V.S. Vassilev, G.A. Haralampiev, *J. Power Sources* 171 (2007) 960–965.
- [15] M. Olper, in: *Eleventh International Lead Conference*, 1993, p. 1993.
- [16] R. David Prengaman, *J. Min. Metals Mater. Soc.* 47 (1995) 31–33.
- [17] J. Yang, R.V. Kumar, D.P. Singh, *J. Chem. Technol. Biotechnol.* 87 (2012) 1480–1488.
- [18] X. Zhu, L. Li, X. Sun, D. Yang, L. Gao, J. Liu, R.V. Kumar, J. Yang, *Hydrometallurgy* 117–118 (2012) 24–31.
- [19] X. Zhu, X. He, J. Yang, L. Gao, J. Liu, D. Yang, X. Sun, W. Zhang, Q. Wang, R.V. Kumar, *J. Hazard. Mater.* 250–251 (2013) 387–396.
- [20] D. Yang, J. Liu, Q. Wang, X. Yuan, X. Zhu, L. Li, W. Zhang, Y. Hu, X. Sun, R.V. Kumar, *J. Power Sources* 257 (2014) 27–36.
- [21] L. Li, Y. Hu, X. Zhu, D. Yang, Q. Wang, J. Liu, R.V. Kumar, J. Yang, *Mater. Res. Bull.* 48 (2013) 1700–1708.
- [22] R. Leibold, F. Huber, *J. Therm. Anal. Calorim.* 18 (1980) 493–500.
- [23] J. Morales, G. Petkova, M. Cruz, A. Caballero, *J. Power Sources* 158 (2006) 831–836.
- [24] Y. Yamamoto, K. Fumino, T. Ueda, M. Nambu, *Electrochim. Acta* 37 (1992) 199–203.
- [25] W. Visscher, *J. Power Sources* 1 (1977) 257–266.